British Geological Survey
NATURAL ENVIRONMENT RESEARCH COUNCIL

Frequency-dependent seismic anisotropy and its implication for estimating fracture size in low porosity reservoirs

Programme: Geochemistry, Mineralogy and Hydrogeology
BGS Research Report CR/03/90N

Enru Liu, Sonja Maultzsch, Mark Chapman, and Xiang Yang Li
British Geological Survey, Edinburgh
John H. Queen, ConocoPhillips, Houston, Texas, USA

British Geological Survey,
Murchison House, West Mains Road,
Edinburgh EH9 3LA, United Kingdom
Tel. 0131 650 0362; Fax. 0131 667 1877
Email. E.Liu@bgs.ac.uk

The full range of Survey publications is available from the BGS Sales Desks at Nottingham and Edinburgh; see contact details below or shop online at www.thebgs.co.uk

The London Information Office maintains a reference collection of BGS publications including maps for consultation.

The Survey publishes an annual catalogue of its maps and other publications; this catalogue is available from any of the BGS Sales Desks.

The British Geological Survey carries out the geological survey of Great Britain and Northern Ireland (the latter as an agency service for the government of Northern Ireland), and of the surrounding continental shelf, as well as its basic research projects. It also undertakes programmes of British technical aid in geology in developing countries as arranged by the Department for International Development and other agencies.

The British Geological Survey is a component body of the Natural Environment Research Council.

Keyworth, Nottingham NG12 5GG

☎ 0115-936 3241 Fax 0115-936 3488
e-mail: sales@bgs.ac.uk
www.bgs.ac.uk
Shop online at: www.thebgs.co.uk

Murchison House, West Mains Road, Edinburgh EH9 3LA

☎ 0131-667 1000 Fax 0131-668 2683
e-mail: scotsales@bgs.ac.uk

London Information Office at the Natural History Museum (Earth Galleries), Exhibition Road, South Kensington, London SW7 2DE

☎ 020-7589 4090 Fax 020-7584 8270
☎ 020-7942 5344/45 email: bgslondon@bgs.ac.uk

Forde House, Park Five Business Centre, Harrier Way, Sowton, Exeter, Devon EX2 7HU

☎ 01392-445271 Fax 01392-445371

Geological Survey of Northern Ireland, 20 College Gardens, Belfast BT9 6BS

☎ 028-9066 6595 Fax 028-9066 2835

Maclean Building, Crowmarsh Gifford, Wallingford, Oxfordshire OX10 8BB

☎ 01491-838800 Fax 01491-692345

Parent Body
Natural Environment Research Council, Polaris House,
North Star Avenue, Swindon, Wiltshire SN2 1EU

☎ 01793-411500 Fax 01793-411501
www.nerc.ac.uk

Contents

Keywords: fracture size estimation, Green's tensor, low porosity reservoir, seismic anisotropy, vertical seismic profile

Executive summary

Frequency-dependent anisotropy has been observed and can be explained by two mechanisms, i.e. seismic scattering by heterogeneities, such as open aligned fractures, and fluid flow in fractured porous rock. If the proper mechanism is understood, it may provide a mean of going beyond the concept of the conventional static equivalent medium theories to potentially estimate size of meso-scale fractures. In this paper, we present some numerical results and synthetic seismograms using the far-field Green's function in fractured porous media. The model that we use takes account of fluid interactions at two scales: meso-scale fractures inserted into a background porous rock with micro-cracks. The fracture lengths can be much larger than grain-scale pores or micro-cracks, but are less than the seismic wavelength, as a result velocity dispersion occurs at the low or seismic frequency, and variation of shear-wave anisotropy with frequency is expected. Our results show that time-delays between split shear-waves vary with fracture sizes: as fracture length increases, shear-wave anisotropy decreases. Our study has indicated the great potential of using seismic anisotropic measurements to estimate fracture sizes, which are critical for fluid flow in fractured rock.

1. Introduction

Fractures are common geological features in the subsurface of the Earth's crust, and they control much of the mechanical strength and transport properties of the solid structure. Fracture systems are also crucial for hydrocarbon production, control and manipulation of water supplies, and dispersal of pollutants. Much of our knowledge about the Earth's crust is obtained from seismic waves. One of the most successful methods for the detection and characterisation of fractures and prediction of fluid flow directions is the use of seismic shear-waves (Crampin 1985; Queen and Rizer 1990, and Li 1997). The success of seismic anisotropy is its ability to provide subsurface fracture orientations as derived from the polarization of fast shear-waves, and spatial distribution of fracture intensity inferred from time-delays between fast and slow shear-waves. However, the reservoir engineers' reluctance to accept seismic anisotropy as a routine technique for fracture characterisation is partially because of its failure to provide information about sizes of fractures. So far the terms 'crack' and 'fracture' have been used as synonyms in geophysics and we do not distinguish between micro-cracks and macro-fractures. Though it has been thought that the presence of micro-scale (grain scale) cracks and/or macro-scale (metre-scale) fractures are both considered to be the dominant causes of observed anisotropy in hydrocarbon reservoirs (Liu et al. 1993), reservoir engineers are more interested in the latter as fluid flow in hydrocarbon reservoirs is believed to be dominated by large-scale fluid units (Queen et al. 1992).

The interpretation of anisotropic measurements made from seismic data requires theoretical models that relate measurable seismic parameters to macroscopically determined rock properties. Based on the assumption that the scalelength associated with fractures is considerably smaller than that of the seismic wavelength, a description of the average properties of a medium will be sufficient. Various equivalent medium theories have been proposed (e.g. Thomsen 1995; Hudson et al. 1996, 2001; Chesnokov et al. 1998; Liu et al. 2000; Parra 2000; Pointer et al. 2000; Tod 2001; van der Kolk et al. 2001; Tod 2001, 2003, b, and Chapman 2003). These theories have provided the foundation for anisotropic analysis, but most theories fail to provide an adequate explanation of velocity dispersion at 'low' or seismic frequency, and it is not possible to determine the size of fractures from seismic data based on those theories. This is because in the conventional equivalent medium theories mentioned above, velocities are given in terms of crack density, a single parameter that depends on both the crack radius and the number density of the cracks.

Recently, strong observational evidence suggests that the measured seismic anisotropy as inferred from time-delays between split shear-waves does actually depend on frequency (Marson-Pidgeon and Savage 1997; Rümpker et al. 1999;

Chesnokov et al. 2001; Liu et al. 2003, and Tod and Liu 2002). Two mechanisms which can introduce velocity dispersion and thus frequency-dependent anisotropy are the scattering of seismic waves in media with preferentially aligned heterogeneities, such as fractures or fine layers, and fluid flow in porous rock. Chapman (2003) and Chapman et al. (2003) present a theoretical model to allow vertically aligned fractures inserted in a porous matrix, where the fractures are much larger than the grain-sized cracks and pores. This model predicts velocity dispersion at 'low' or seismic frequencies and can well explain the observed frequency-dependent seismic anisotropy. A similar model using the method of smoothing has been developed by Tod (2003). This latest advance in theoretical developments provides a theoretical basis to potentially determine fracture sizes from remotely measured seismic attributes.

In this study, we use the model proposed by Chapman (2003) to examine the variation of anisotropy with frequency, in particular, we restrict ourselves to seismic frequency ranges. In Section 2, we present the anisotropic Green's function, which can handle frequency-dependent elastic stiffness. This is followed by a brief introduction Section 3 to the model of Chapman (2003). In Section 4, we present 4-component synthetic seismograms using the full-space far-field Green's function, and apply the rotation technique to the synthetic data. We show that the shear-wave anisotropy varies with fracture sizes, i.e. the time-delays between split shear-waves decrease systematically as fracture size increases, which agrees with the observation. In Section 5, modelling results for a field VSP dataset analysed by Liu et al. (2003) are presented to demonstrate the effectiveness of the model of Chapman (2003). Finally, the possibility of estimating fracture sizes from seismic anisotropy measurements is discussed in Section 6.

2. Green's tensors in general anisotropic media

The fundamental solution or the Green's function in general anisotropic media has continued to be of great interest to researchers in fields involving wave propagation. However, rather surprisingly, progress has been very slow in deriving a method to evaluate the Green's function efficiently. In this section, we present an analytic expression of the Green's function for the far field. It is derived in the frequency-domain, and can handle frequency-dependent elastic moduli.

We consider the equation of motion for a 3D elastic homogenous anisotropic medium when an arbitrary body force is applied,

$$\rho\omega^2 u_i(\vec{x}) - C_{ijkl}\frac{\partial^2 u_l(\vec{x})}{\partial x_j \partial x_k} = F_i(\vec{x}')\delta(\vec{x}-\vec{x}'), \qquad (1)$$

where u_i is the ith component displacement at $\vec{x}$, F_i is the ith component of the applied body force at $\vec{x}'$, ρ is density, C_{ijkl} are the elements of the uniform elastic coefficient tensor (in general anisotropic media there are 21 elastic coefficients), and $\delta(\vec{x})$ is the Dirac delta function. Einstein summation convention is understood throughout this section. The solution to equation (1) is given by the convolution of the Green's tensor and the applied body source, i.e.

$$u_i(\vec{x}) = G_{ij}(\vec{x}, \vec{x}')F_j(\vec{x}') \ , \tag{2}$$

where Green function $G_{ij}(\vec{x}, \vec{x}')$ is given in the following integral form by Burridge (1967) using our notation,

$$G_{ij}(\vec{x}, \vec{x}') = -\frac{1}{4\pi\rho}\sum_{n=1}^{3}\int_{S(\vec{p})} dS(\vec{p})\frac{g_i^{(n)}g_j^{(n)}}{w^{(n)}}\exp(ik^{(n)}r), \tag{3}$$

for the ith displacement at point $\vec{x}$ due to the application of a unit force in the jth direction at point $\vec{x}'$. $r = |\vec{x} - \vec{x}'|$ is the distance of the receiver at $\vec{x}$ from the source at $\vec{x}'$. $\vec{p} = \{p_i\}$ is the slowness vector, $k^{(n)} = v^{(n)}/\omega$ is wavenumber, ω is frequency, $v^{(n)}$ is the phase velocity of the nth wave, $w^{(n)}$ is the group velocity of the nth wave, $g_i^{(n)}$ is ith component of the polarization vector of the nth wave, and $S(\vec{p})$ is the slowness surface. In anisotropic media, there are in general three distinct waves travelling at different speeds (see below), resulting in the summation in equation (3).

The integral in equation (3) is difficult to evaluate and generally not useful for practical implementation. There have been many attempts to compute this integral efficiently, surprisingly even very recently. Various assumptions have to be used, even in the simplest case of transversely isotropic (TI) media, where as in isotropic media, the *SH*-wave is de-coupled from *P*- and *SV*-waves. Dong and Schmitt (1994) provide an expression of the Green's function in TI media in the form of inverse Laplacian transform. Sáez and Domínguez (2000) consider only the case of elliptical anisotropy (i.e. assuming *P*-wave wavefront is elliptical, resulting in *SV*-wave wavefront being simply circular). For weak TI media, Vavryčuk (1997) derives far-field Green's function based on ray solutions. Gridin (2000) has provided an analytic solution for the far-field Green's function in TI media at shear-wave singularities. For general anisotropic media, progress was not made until the Radon transform form of equation (3) was derived by Wang and Achenbach (1994, 1995) and numerically evaluated by the authors themselves and more recently by Dravinski and Zheng (2000). Though the anisotropic Green's function in the form of the Radon transform is simpler than the integral form of equation (3), it is still not easy to evaluate numerically, particularly for implementation in boundary element methods where Green's function has to be integrated for each segment. Fortunately, in most seismological applications, the near-field solution is not needed, and the far-field solution is usually sufficient. Following

Ben-Menahem and Gibson (1990, 1995); Benahem and Sena (1990); Kendall et al (1992), and Gajewski (1993), the far-field or ray solution of the Green tensor is given by,

$$G_{ij}(\vec{x},\vec{x}',\omega) = \mp\frac{1}{4\pi\rho r}\sum_{n=1}^{3}\frac{g_i^{(n)}g_j^{(n)}}{w^{(n)}\sqrt{K^{(n)}}}\exp(ik^{(n)}r), \tag{4}$$

where $K^{(n)}$ is the Gaussian curvature of the slowness surface of the nth wave, and a procedure for computing K is given by Gajewski (1993). The plus sign is used when the larger of the principal curvature of the slowness surface is negative, and the minus sign when the principal curvature is positive. For completeness, we also give the corresponding traction Green tensor which is related to the Green displacement tensor by Hooke's law,

$$T_{ij}(\vec{x},\vec{x}') = C_{ipkl}n_p\frac{\partial G_{kj}(\vec{x},\vec{x}')}{\partial x_l} = \pm C_{ipkl}n_p(\vec{x})\frac{i}{4\pi\rho}\sum_{n=1}^{3}\frac{g_k^{(n)}g_j^{(n)}p_l^{(n)}}{w^{(n)}\sqrt{K^{(n)}}}\exp(ik^{(n)}r), \tag{5}$$

for the traction in the ith direction at point $\vec{x}$ on the boundary due to the application of a unit force in the jth direction at point $\vec{x}'$. $\{n_i\}$ is the normal at receiver position $\vec{x}$. Note that the traction Green's function is needed in the formulation of boundary element methods. The phase velocities $\{v_i\}$ and polarization vector $\{g_i\}$ can be obtained by solving the Kevin-Christoffel equation,

$$\left|C_{ijkl}n_jn_k - \rho v^2\delta_{jk}\right| = 0. \tag{6}$$

There are in general three complex eigenvalues with three orthogonal eigenvectors. The three eigenvalues are the phase velocities, and the corresponding three eigenvectors are the polarization vectors of the three body waves. The group (energy or ray) velocities $\{w_i\}$ can be calculated by,

$$w_i = \left(C_{ijkl}/\rho\right)p_lg_jg_k. \tag{7}$$

Equations (4) and (5) cannot be applied in a vicinity of parabolic points of the slowness surfaces at which K=0. In isotropic media, the Gaussian curvature K of the slowness surface is simply the square of the phase velocity of the corresponding wave, and the phase velocity equals to group or ray velocity, i.e. $\vec{v} = \vec{w}$. Equations (4) and (5) reduce to the far-field Green functions for isotropic media.

In the 2D case, the Hankel functions replace the exponential functions (with the use of the Weyel integral), i.e. $\frac{e^{ikr}}{r} \to H_0^{(1)}(kr)$ (for displacement) and $\frac{ie^{ikr}}{r} \to H_1^{(1)}(kr)$ (for traction). $H_0^{(1)}$ and $H_1^{(1)}$ are the zeroth and first-orders respectively of Hankel functions of the first kind.

The elastic stiffness C_{ijkl} can be complex and frequency-dependent, resulting in complex eignvalues from Christoffel equation (6), with the real part giving the velocity, and imaginary part giving the attenuation. The inverse of the quality factor is given by

$$Q^{-1} = 2\frac{\mathrm{Im}(k)}{\mathrm{Re}(k)} = 2\frac{\mathrm{Re}[v(\omega)]}{\mathrm{Im}[v(\omega)]}, \tag{8}$$

for given phase velocity $\{v_i\}$ and frequency ω.

Gajewski (1993) did a detailed study of the radiation patterns of various sources using equation (4), which will not be repeated here. Instead, we only show one synthetic example to demonstrate of the validity of our implementation. Figures 1 and 2 show the comparison of the synthetic seismograms for an isotropic full space computed using the isotropic and anisotropic Green's functions. In the model, we use a vertical force and a 30Hz Ricker wavelet. The source is at the origin with five receivers at the positions of (0.2, 0.3), (0.2, 0.6), (0.2, 0.9), (0.2, 1.2) and (0.2, 1.5) km. We can see that in general isotropic and anisotropic solutions give identical results in the limit of isotropy, and the differences are marginal.

3. Effective elastic stiffness of porous rock with meso-scale fractures

In this Section, we summarise the model developed by Chapman (2003) to model macro-fractures in porous rocks with isotropic distribution of random micro-cracks. The merits and limitations are discussed in Chapman et al. (2003). The effective elastic stiffness tensor is written as

$$C = C_0 - \phi C_1 - e_c C_2 - e_f C_3, \tag{9}$$

where ϕ is porosity of the matrix, e_c is the density of micro-cracks, and e_f is the density of macro-fractures. C_0 is the elastic stiffness of the matrix, C_1, C_2 and C_3 are the contributions of pores, cracks and fractures, respectively, and their explicit expressions are given in the Appendix of Chapman et al. (2003). The size-dependent terms of elastic stiffness are linked by the relationship between two relaxation time scales, τ_m and τ_f, i.e. $\tau_f = \left(\frac{a_f}{a_m}\right)\tau_m$, where τ_m is related to the standard micro-structural squirt flow and τ_f is related to the meso-scale flow due to the presence of fractures. a_f is the fracture radius, and a_m is the grain size (the size of pores and micro-cracks). Note that a_f can be much larger than a_m. The frequency-dependent terms are governed by two terms: $\left(1+i\omega\tau_f\right)^{-1}$, which is related to fluid flow into and out of fractures, and $\left(\frac{1+i\omega\gamma\tau_m}{1+i\omega\tau_m}\right)^{-1}$, which is related to pore-scale flow (γ is related to the Poisson' ratio of the matrix and the fluid compressibility). In the absence of fractures the model returns to the grain-scale squirt

flow model. With the introduction of a fracture set two characteristic frequencies exist: the traditional squirt flow frequency which can be estimated from laboratory data, together with a lower characteristic frequency which depends on the size of the fractures. A consequence of this is that propagation at seismic frequencies can be very different from that predicted in the low frequency limits, such as used in Thomsen (1995), implying that dispersion can occur at seismic frequency, or in other words seismic frequency can no longer be safely regarded as the low frequency limit.

Using simple algebra, we can obtain expressions of elastic stiffness in terms of Thomsen's parameters, or in terms of fracture compliance as used in Liu et al. (2000). Figure 3 shows the variation of three Thomsen's anisotropic parameters with frequency computed for different fracture sizes. The following parameters have been used in our examples: V_P=3.5 km/s, V_S=2 km/s, ρ=2.3 g/cm^3, e_c=0.04, e_f=0.04, porosity ϕ =10%, and the relaxation time τ_m=10^{-7} (gas). The fracture sizes are indicated on each individual plot. We use f=30 Hz in all cases except where stated otherwise which gives a *P*-wave wavelength of λ_P=116 m, and λ_S=66 m, and a Ricker wavelet is used in all synthetics. We can see that as the fracture size increases, or equivalently frequency increases, all Thomsen's three parameters decrease, implying anisotropy decreases. When the size of aligned fractures are in the same order of pores and micro-cracks, there is little dependence of anisotropy parameters on frequency (i.e. the model reduces to the static or zero frequency equivalent medium theory). Figure 4 shows the variation of attenuation with azimuth for *qP*- and *qSV*-waves for different fracture sizes. Figures 5 and 6 show the comparison of synthetic seismograms of the horizontal (Figure 5) and vertical (Figure 6) components for the fracture lengths of 0.1m (solid lines) and 5m (dashed line). We can clearly the dependence of attenuation and amplitudes on fracture sizes, suggesting that by careful analysis it should be possible to infer information about the fracture sizes from attenuation anisotropy and amplitude information, such as AVO. This is currently under investigation.

4. Synthetic examples

We generate synthetic seismograms using the anisotropic Green's function (Section 2) and the complex elastic stiffness from Chapman's (2003) model described in Section 3. The more appropriate method would be to modify the reflectivity method to allow frequency-dependent elastic stiffness. The model is a VSP geometry with an offset of 0.1km, with 100 receivers located at depths of between 0.1km and 2km (spacing is 0.02km). Two horizontal component sources which generate shear-waves are used and the source is Ricker wavelet with a peak frequency of 30Hz. The fractures have a length of 5m, and are oriented 60^o from the X-direction with a 10^o dip. The upper panel of Figure 7 displays the horizontal four-component data matrix from the in-line (*SV*)

and cross-line (*SH*) sources. The top rows marked with XX and XY are from in-line (*SV*) sources, and the bottom rows marked with YX and YY are from cross-line (SH) sources. The first letter denotes the source orientation, and the second the receiver orientation. The data are displayed with relative true amplitudes so that a direct comparison between different components can be made. We can immediately see that there is strongly coupled energy in the cross-components, i.e. energy from the in-line source is recorded in the cross-line receiver (XY) and energy from the cross-line source is recorded in the in-line receiver (YX). This feature is a direct consequence of the presence of azimuthal or fracture-induced anisotropy. Conventional analysis of multicomponent shear-wave data involves simple rotation of horizontal four-component shear-wave data into the natural co-ordinate through the use of standard methods such as Alford rotation (Alford 1986), or the linear transform (Li and Crampin 1993) with the aim of separating the two split shear-waves by minimising the off-diagonal energy. The rotated four-component data are displayed in the lower panel of Figure 7, which shows clearly that the off-diagonal energy has been significantly reduced. Once the shear-wave data are rotated into natural co-ordinate systems, the fast and slow shear-waves are separated. The rotation angle then represents the polarization angles of the fast split shear-waves, which are interpreted as the fracture orientation. A cross-correlation can be applied to the fast and slow components to obtain the time-delays between the two split shear-waves. Figure 8 shows the polarization angles obtained for three models with different fracture lengths of 1m, 5m, and 10m. Except for the shallow receivers, the polarizations are generally constant at 60^o, which is very close to the direction of fracture orientation used in the models, and the small difference up to 2^o is due to the 10^o dip in the fracture orientation. Figure 9 shows the variations of time-delays between fast and slow shear-waves. We can immediately see that as receiver depth increases, time-delays increase linearly. More important for the purpose of the present study is the clear variation of time-delays with fracture length or frequency. As fracture size decreases or equivalently frequency increases, time-delay decreases, similar to the observed variation in Liu et al. (2003).

5. Estimating fracture size from VSP data

We apply the model of Chapman (2003) to estimate fracture density and fracture size from 9C VSP data from the Bluebell Altamont field in the Uinta basin, Utah. The field contains a fractured gas reservoir, the Green River formation, which has in general low porosity and permeability. Production from the reservoir is believed to be primarily controlled by size, orientation and concentration of natural fractures (Lynn et al. 1999). Therefore it is vital to obtain estimates of these parameters from seismic data.

Analysis of the VSP data for frequency dependent anisotropy is discussed in Liu et al. (2003). It was found that the time-delay between the split shear waves measured in the Green River formation systematically decreases with frequency over a frequency band of 5 to 40 Hz. Here we propose a new method to estimate the fracture size in addition to fracture orientation and density from the shear wave data.

The model was first simplified as discussed in Chapman et al. (2003) and calibrated with laboratory data from Rathore et al. (1995). As a result we may obtain an estimate of the time-scale parameter τ_m for microscopic fluid flow. Then we apply petrophysical corrections according to rock and fluid properties of the Green River formation to the τ_m-value, so that it may be used as a defined input parameter for our modelling. The remaining two fitting parameters are the fracture density and the fracture radius. The inversion for those two parameters comprises the following steps:

- Measuring the time-delay over a depth interval for various frequency bands from the VSP data.
- Scanning through a range of fracture densities and sizes, computing the predicted time-delay over depth for each centre frequency of the chosen frequency bands.
- Computing the RMS error over all centre frequencies for each pair of fracture density and fracture radius.
- Finding the minimum of the error function.

Figure 10 shows the computed relative error over a large range of fracture densities and sizes. We can see that there is a well-defined minimum around a fracture radius of 1.5 m and a fracture density of 0.038, where the error is less then 5%. The plot also demonstrates that there are considerable differences in estimated fracture density between a high frequency model such as Hudson's (1981) (upper end of the figure) and a low frequency model such as Thomsen's (1995) equant porosity model (lower end of the figure). Figure 11 displays the same plot as Figure 10 zoomed into the region of the minimum. We find a fracture density of 0.0375 and a fracture radius of 1.34 m for the minimum relative error.

We use those values to compute frequency dependent elastic coefficients for the Green River formation and build a 1D-model for the computation of synthetic seismograms. The fractures in the model are striking N43W as found from the real data, and they are rotated 20º off the vertical plane. We use a new version of the full wave modelling program ANISEIS®, which can handle frequency dependent elastic coefficients, to compute synthetic seismograms.

Figure 12 and 13 show the inline and crossline components from the real data in comparison with the synthetic seismograms for the Green River formation,

respectively. The synthetic data are then processed in the same way as the real data (see Liu et al. 2003). The fast and slow shear waves are separated by performing a 4-component Alford rotation. We filter the data into different frequency bands to estimate polarization angles and time-delays.

Figure 14 shows the polarization angle of the S_1 waves (the fast shear waves) for the chosen frequency bands over the depth interval of the Green River formation. They have a constant value of around 44º, which departs from the angle of the fracture strike by 1º because of the dip of the fractures. Figure 15 displays the time-delays obtained for each frequency range from the synthetic data (solid lines). For comparison, the dashed lines show the time-delays found in the real data. The modelling results show very good agreement with the real data. In general the slopes of the lines corresponding to the synthetic data are slightly lower and the error appears to be higher at low frequencies. In other words, the change of time-delays with frequency and the anisotropy are slightly smaller than that estimated from real data. However, in terms of the parameter of interest, the fracture radius, the error in the results only corresponds to a change of about 20 cm, which is not significant.

It is the aim of future work to clarify what causes the slight differences between the results and to establish a revised and accurate procedure for the inversion. In the above method we assume the time-delays for each frequency band to be representative for the centre frequency of that band. It is, however, some kind of average of the time-delays for all frequencies contained in the data, weighted by the frequency spectra of the source wavelet and the bandpass filter. Since the change in anisotropy with frequency is not linear, that average will not correspond to the time-delay of the centre frequency of a particular band. The time frequency analysis proposed by Liu et al. (2003) will probably be an appropriate method to obtain input data for the inversion. It is desirable to define the frequency dependence of anisotropy with more than four frequency values, especially in the range where the time-delay changes very rapidly with frequency. An error and sensitivity analysis will also be necessary.

Although the details of the inversion and the processing are still to be defined, we have already obtained a very satisfactory result. The estimated fracture radius of 1.34 m (or fracture length of 2.68 m) corresponds to fracture lengths observed in cores and FMS images, which extended 2 to 3 m into the vertical/sub-vertical direction. The estimated fracture density of 0.0375 lies in the middle of the values that would be obtained by using Thomsen's (1995) and Hudson's (1981) models, respectively. Analysing frequency dependent anisotropy using the model of Chapman (2003) allows us not only to obtain an improved estimate of the fracture density, but also to measure a fracture length, which is of great interest for the description of reservoirs and which enables us to discriminate between fracture and non-fracture induced anisotropy.

6. Discussion on potential of estimating fracture sizes from seismic anisotropy

The application of seismic anisotropy is so far limited by the necessary theoretical constraints of dilute concentrations and very small scale-size to wavelength ratios, as heterogeneous and fractured porous rock may be characterised by observations in different critical wavelength ranges, each reflecting different physical mechanisms. This limitation has not been satisfactorily addressed until very recently (see references cited in the Introduction). The observations of frequency-dependent anisotropy by Marson-Pidgeon and Savage (1997); Chesnokov et al. (2002), and Liu et al. (2003) provide a new challenge to theoreticians. Note that change in shear-wave polarizations has been reported by Fouch and Fischer (1998), and they interpret this as different responses of shear-waves to different alignments with different scales in the rock-mass. If two scales are present, say, micro-cracks are aligned in different directions from aligned macro-fractures, low frequency would expect to give polarization of macro-fractures, and high frequency would give direction of micro-cracks, however such a model is not yet available. The nearest analogue is the combination of two crack sets (conjugate fracture sets), which has been studied by Liu et al. (1992). It was found that polarization of the fast split shear-wave would give a crack-density weighted average direction between the conjugate sets. It would be interesting to extend the model of Chapman (2003) to allow aligned micro-cracks and aligned fractures in different directions.

Scattering of seismic waves has long been recognised to be frequency-dependent (e.g. Leary and Abercrombie 1994, Wu 1981). It has also been realised that heterogeneities will produce apparent anisotropy. Shapiro et al. (1994), and Werner and Shapiro (1999) demonstrate that anisotropy differs for waves with different frequencies in finely-layered media. This leads to the conclusion that any heterogeneous material with a certain alignment or an ordered distribution must behave like an anisotropic medium to elastic waves at some frequencies. The presence of a heterogeneous medium can produce frequency-dependent anisotropy, in which the influence of heterogeneities decreases as frequency increases. The scale of heterogeneities needs to be small enough to cause effective anisotropy instead of scattering. This requires a quasi-homogeneous propagation regime which can be expressed mathematically as $ka < 0.1$, where k is the wavenumber, and a is the scalelength of the heterogeneities.

The model of Chapman (2003) and Chapman et al. (2003) as used in this paper assumes a set of aligned meso-scale fractures in porous media. The fractures can be much larger than the cracks and pores, but are much smaller than the wavelength. This is in contrast to the early models of Hudson et al. (1996) and Thomsen (1995) as discussed in Hudson et al. (2001). Coupled fluid flow motion occurs on two scales: the grain scale and the scale of the fractures. A consequence of this is that the predicted

anisotropy becomes frequency-dependent, with the form of the dependence related directly to the fracture size. Previous estimates of the squirt flow frequency have given high values, typically between the sonic and ultrasonic bands, which leads to the suggestion that at seismic frequencies there should be little dispersion. In the presence of larger scale fractures, substantial frequency dependence can be expected in the seismic frequency ranges, and therefore it is not safe to treat seismic frequency as a low frequency limit. The percentage of anisotropy change can be up to 5 to 10% for gas filled, and 2% for brine-filled fractures. Note that an alternative model has been developed by Tod (2003) as used by Tod and Liu (2002) in which a fluid flow mechanism between elliptical cracks (bed-limited cracks) is proposed. This model produces a frequency-dependence in the resulting effective material parameters, and hence in the shear-wave splitting. The models of Chapman (2003) and Tod (2003, b) have at least one feature in common, that is the significance of the effects of multi-scale fluid flow is emphasised in contrast to the wave scattering which earthquake seismologists prefer to use.

Multi-scale fluid interaction resulting in frequency-dependent anisotropy is a very interesting phenomenon. We argue that both scattering and fluid-flow may contribute to observed frequency-dependent anisotropy. However, we suggest that meso-scale fractures in porous rocks are more likely to be the dominant cause in at least fractured hydrocarbon reservoirs. Our study has an important implication for characterisation of natural fractures in that fracture sizes, which control the fluid flow, may potentially be predicted from seismic anisotropic measurement (note that metre-scale fractures are normally regarded as fluid flow units by reservoir engineers). In other words, we may potentially go beyond the static equivalent medium theories to extract information about fracture sizes and fluid properties in addition to fracture orientation and fracture density.

7. Conclusions

We have presented results demonstrating the dependence of seismic anisotropic parameters on frequency using the model of Chapman (2003). We also show synthetic seismograms using far-field analytic expressions of Green's function in anisotropic media. We emphasise the wave dispersion at low frequency, and have therefore restricted ourselves to seismic frequency bands in all examples. Our results can explain observed variation of shear-wave anisotropy with frequency in terms of multi-scale fluid flow in fractured porous rock. Synthetic seismograms and modelling of real VSP data reveal the variation of time-delays between split shear-waves with fracture size, and that as fracture length increases or frequency increases, shear-wave anisotropy decreases. Our study has indicated the great potential of using anisotropy measurements to estimate the fracture sizes, which are ultimately needed in reservoir simulation. In the

future, we still need to investigate this model further to better understand the effects of multi-scale fractures on AVO, FVO (frequency variation with offset as used in Lynn et al. 1999, and Shen et al. 2002), and attenuation anisotropy on AVO. We will pay particular attention to see how *P*-waves can be used to estimate fracture sizes.

Acknowledgements

We thank John Hudson and Simon Tod (Cambridge Univ.), Kurt Nihei, Seiji Nakagawa, Larry Myer and Ernest Majer (Lawrence Berkeley Lab.), Heloise Lynn (Lynn Inc.), Evgeni Chesnokov (Oklahoma Univ.), Greg Ball (ChevronTexaco) and Mike Kendall (Leeds Univ.) for useful discussions on various occasions. We also thank Larissa Fradkin (South Bank Univ.) for sending reprints on Green's function, and our colleagues David Booth and Tony Milodowski for comments on this report. Part of this work was supported by the sponsors of Edinburgh Anisotropy Project, and is published with the approval of the Executive Director of the British Geological Survey (NERC).

References

Alford, R.M. 1986. Shear data in the presence of azimuthal anisotropy, Dilley, Texas. *56th Ann. Internat. Mtg., Soc. Explor. Geophys., Expanded Abstracts,* 476-479.

Ben-Menahem, A. and Gibson, R.L. 1990. Elastodynamic Green's tensor and radiation patterns of point sources in general anisotropic inhomogeneous media. *Geophys. J. Int.* **107**, 297-308.

Ben-Menahem, A. and Gibson, R.L. 1995. Radiation of elastic waves from sources embedded in anisotropic inclusions. *Geophys. J. Int.* **122**, 249-265.

Ben-Menahem, A. and Sena, A.G. 1990. Seismic source theory in stratified anisotropic media. *J. Geophys. Res.* **95**, 15,395-15,427.

Burridge, R. 1967. The singularity on the plane lids of the wave surface of elastic media with cubic symmetry. *Q. J. Mech. Appl. Math.* **20**, 41-56.

Chapman, M. 2003. Frequency dependent anisotropy due to meso-scale fractures in the presence of equant porosity. *Geophys. Prosp.,* In press.

Chapman, M., Maultzsch, S., Liu, E. and Li, X.Y. 2003. The effect of fluid saturation in an anisotropic, multi-scale equant porosity model. *J. Appl. Geophys.*, In press.

Chesnokov, E.M., Kukharenko, Yu. A. and Kukharenko, P.Yu. 1998. Frequency-dependence of physical parameters of microinhomogeneous media: Space statistics. *Revue de L'Institut Francais du Petrole* **53**, 729-734.

Chesnokov, E.M, Queen, J.H., Vichorev, A., Lynn, H.B, Hooper, J., Bayuk, I., Castagna, J. and Roy, B. 2001. Frequency dependent anisotropy, *71st Ann. Internat.*

Mtg: Soc. of Expl. Geophys., Expanded Abstracts, 2120-2123.

Crampin, S. 1985. Evaluation of anisotropy by shear-wave splitting. *Geophysics* **50**, 142-152.

Dong, W. and Schmitt, D. 1994. Simplified dynamic and static Green's functions in transversely isotropic media. *Geophys. J. Int.* **119**, 231-242.

Dravinski, M. and Zheng, T. 2000. Numerical evaluation of three-dimensional time-harmonic Green's functions for a nonisotropic full-space. *Wave Motion* **32**, 14-151.

Fouch, M.J. and Fischer, K.M. 1998. Frequency-dependent shear-wave anisotropy in the Mariana subduction zone. *EOS Trans. AGU Suppl., 79, S212.*

Gajewski, D. 1993. Radiation from point sources in anisotropic media. *Geophys. J. Int.* **113**, 299-317.

Gridin, D. 2000. Far-field asymptotics of he Green's tensor for a transversely isotropic solid. *Proc. R. Soc. Lond.* **A456**, 572-591.

Hudson, J.A., 1980. Overall properties of a cracked solid. *Mathematical Proceedings of Cambridge Philosophy Society* **88**, 371-384.

Hudson, J., Liu, E. and Crampin, S. 1996. The mechanical properties of materials with interconnected cracks and pores. *Geophys. J. Int.* **124**, 105-112.

Hudson, J., Pointer, T. and Liu, E. 2001. Effective medium theories for fluid-saturated materials with aligned cracks. *Geophys. Prosp.* **49**, 509-522.

Kendall, J.-M., Guest, W.S. and Thomson, C.J. 1992. Ray-theory Green's function reciprocity and ray-centred co-ordinates in anisotropic media. *Geophys. J. Int.* **108**, 364-371.

Leary, P. and Abercrombie, R. 1994. Frequency dependent crustal scattering and absorption at 5-160 Hz from coda decay observed at 2.5 km depth. *Geophys. Res. Lett.* **21**, 971-974.

Li, X.Y. 1997. Fractured reservoir delineation using multicomponent seismic data. *Geophys. Prosp.* **45**, 39-64.

Li, X.Y. and Crampin, S. 1993. Linear transform techniques for analysing split shear-waves in four-component seismic data. *Geophysics* **58**, 240-256.

Liu, E., Crampin, S., Queen, J. H. and Rizer, W.D. 1992. Behaviour of shear-waves in rocks with two sets of cracks. *Geophys. J. Int.* **113**, 509-517, 1992.

Liu, E., Crampin, S., Queen, J.H. and Rizer, W.D. 1993. Velocity and attenuation anisotropy caused by micro-cracks and macro-fractures in a multiazimuthal reverse VSP. *Can. J. Explor. Geophys.* **29**, 177-188.

Liu, E., Hudson, J.A. and Pointer, T. 2000. Equivalent medium representation of fractured rock. *J. Geophys. Res.* **105**, 2981-3000.

Liu, E., Queen, J.H., Li, X.Y., Chapman, M., Lynn, H.B. and Chesnokov, E.M. 2003. Analysis of frequency dependent seismic anisotropy from a multicomponent VSP. *J. Appl. Geophys.*, in press.

Lynn, H. B., Beckham, W. E., Simon, K. M., Bates, C. R., Layman, M. and Jones, M. 1999. *P*-wave and S-wave azimuthal anisotropy at a naturally fractured gas reservoir, Bluebell-Altamont Field, Utah. *Geophysics* **64**, 1293-1311.

Marson-Pidgeon, K. and Savage, M.K. 1997. Frequency-dependent anisotropy in Wellington, New Zealand. *Geophys. Res. Lett.* **24**, 3297-3300.

Parra, J.O. 2000. Poroelastic model to relate seismic wave attenuation and dispersion to permeability anisotropy. *Geophysics* **65**, 202-210.

Pointer, T., Liu, E., Hudson, J.A. 2000. Seismic wave propagation in cracked porous media. *Geophys. J. Int.* 142, 199-131.

Queen, J.H. and Rizer, W.D. 1990. An integrated study of seismic anisotropy and the natural fracture systems at the Conoco Borehole Test Facility, Kay County, Oklahoma. *J. Geophys. Res.* **95**, 11255-11273.

Queen, J.H., Rizer, W.D. and DeMartini, D. 1992. Geophysical methods of fracture detection and estimation. *The Leading Edge* 19-21, January 1992.

Rathore, J.S., Fjaer, E., Holt, R.M. and Renlie, L., 1995. P- and S-wave anisotropy of a synthetic sandstone with controlled crack geometry. *Geophysical Prospecting* **43**, 711-728.

Rümpker, G., Tommasi, A. and Kendall, J.-M. 1999. Numerical simulations of depth-dependent anisotropy and frequency-dependent wave propagation effects. *J. Geophys. Res.* **104**, 23,141-23,153.

Sáez, A. and Domínguez, J., 2000. Far-field dynamic Green's functions for BEM in transversely isotropic solids. *Wave Motion* **32,** 113-123

Shapiro, S.A., Zien, H. and Hubral, P. 1994. A generalised O'Doherty-Ansley formula for waves in finely layered media. *Geophysics* **59**, 1750-1762.

Shen, F., Sierra, J., Burns, D.R. and Toksöz, M.N. 2002. Azimuthal offset-dependent attributes applied to fracture detection in a carbonate reservoir. *Geophysics* **67**, 355-364.

Tod, S.R. 2001. The effects on seismic waves of interconnected nearly aligned cracks. *Geophys. J. Int.* 146, 249-263

Tod, S.R. 2003. Bed-limited cracks in effective medium theory. *Geophys. J. Int.*, **152**, 244-352.

Tod, S.R. 2003. Effective medium theory for cracked poroelastic media using the method of smoothing. *Geophys. J. Int*., submitted.

Tod, S.R. and Liu, E. 2002. Frequency-dependent anisotropy due to fluid flow in bed-limited cracks. *Geophys. Res. Lett.*, **29**, No.15, Paper No.10.1029/2002GL015369

Thomsen, L. 1995. Elastic anisotropy due to aligned cracks in porous rock. *Geophys. Prosp.* **43**, 805-829.

van der Kolk, C.M., Guest, W.S. and Potters, J.H.H.M., 2001. The 3D shear experiment over the Natith field in Oman: the effect of fracture-filling fluids on shear-wave

propagation. *Geophys. Prosp.* **49**, 179-197.

Vavryčuk, V. 1997. Elastodynamic and elastostatic Green tensors for homogeneous weak transversely isotropic media. *Geophys. J. Int.* **130**, 786-800.

Wang, C.Y. and Achenbach, J.D. 1994. Elastodynamic fundamental solutions for anisotropic solids. *Geophys. J. Int.* **118**, 384-392.

Wang, C.Y. and Achenbach, J.D. 1995. Three-dimentional time-harmonic elastodynamic Green's functions for anisotropic solids. *Proc. R. Soc. Lond.* **449**, 441-458.

Werner, U. and Shapiro, S.A. 1999. Frequency-dependent shear-wave splitting in thinly layered media with intrinsic anisotropy. *Geophysics* **64**, 604-608.

Wu, R.S. 1981. Attenuation of short period seismic waves due to scattering. *Geophys. Res. Lett.* **9**, 9-12.

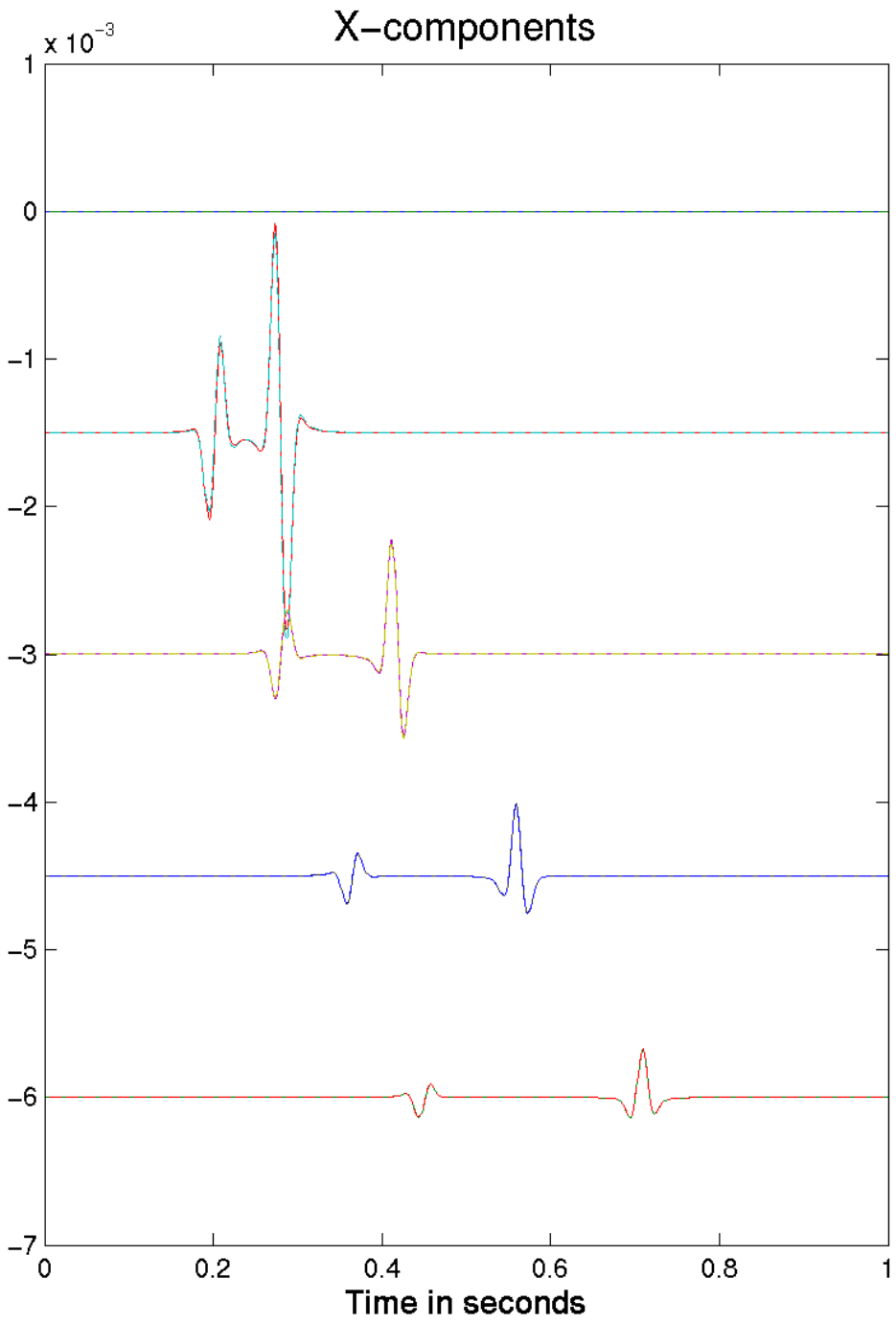

Figure 1. Comparison of synthetic seismograms of the horizontal components computed using the isotropic Green's function (solid lines) and anisotropic Green's function (dashed line). The isotropic model is described in the text.

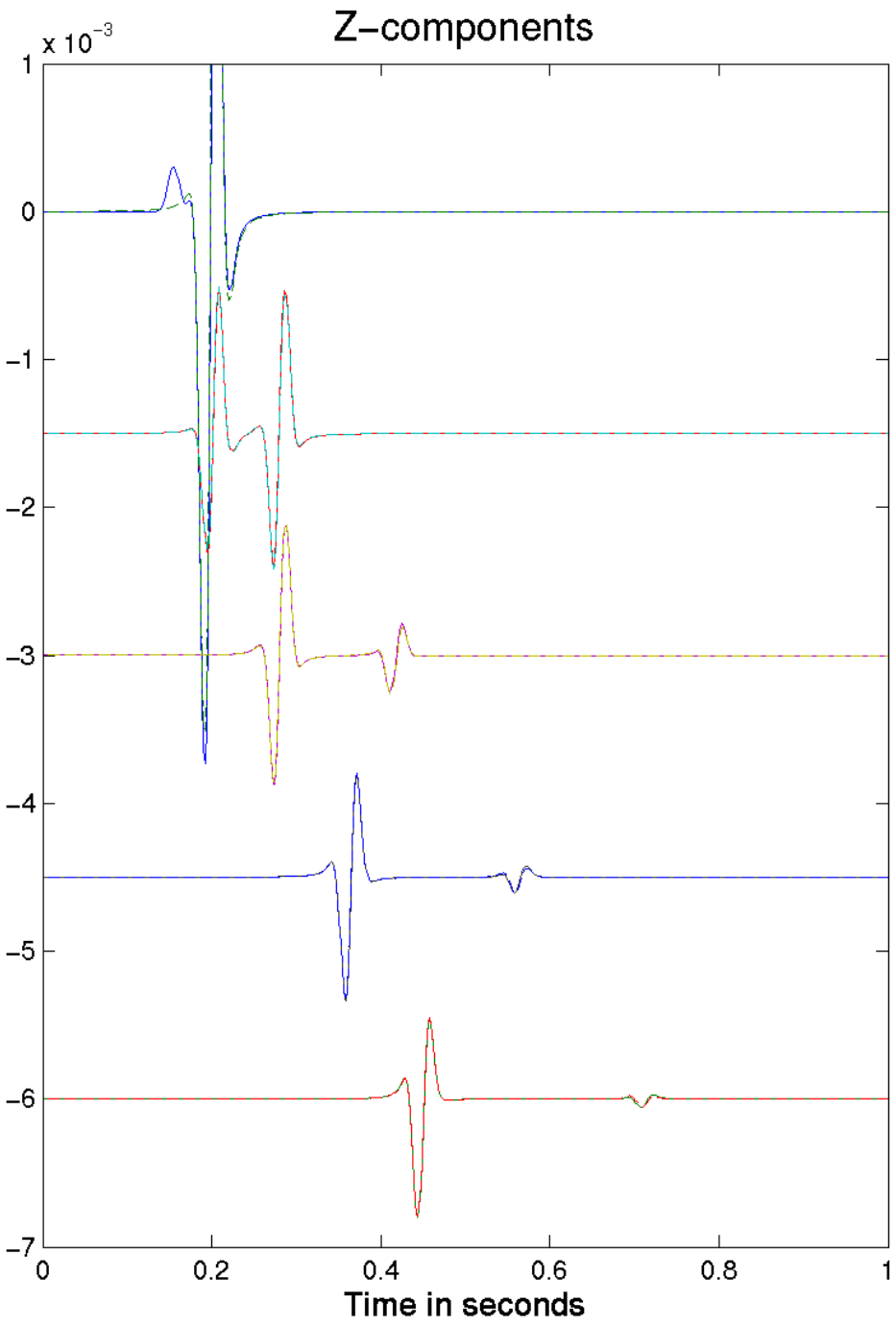

Figure 2. Comparison of synthetic seismograms of the vertical components computed using the isotropic Green's function (solid lines) and anisotropic Green's function (dashed line). The isotropic model is described in the text.

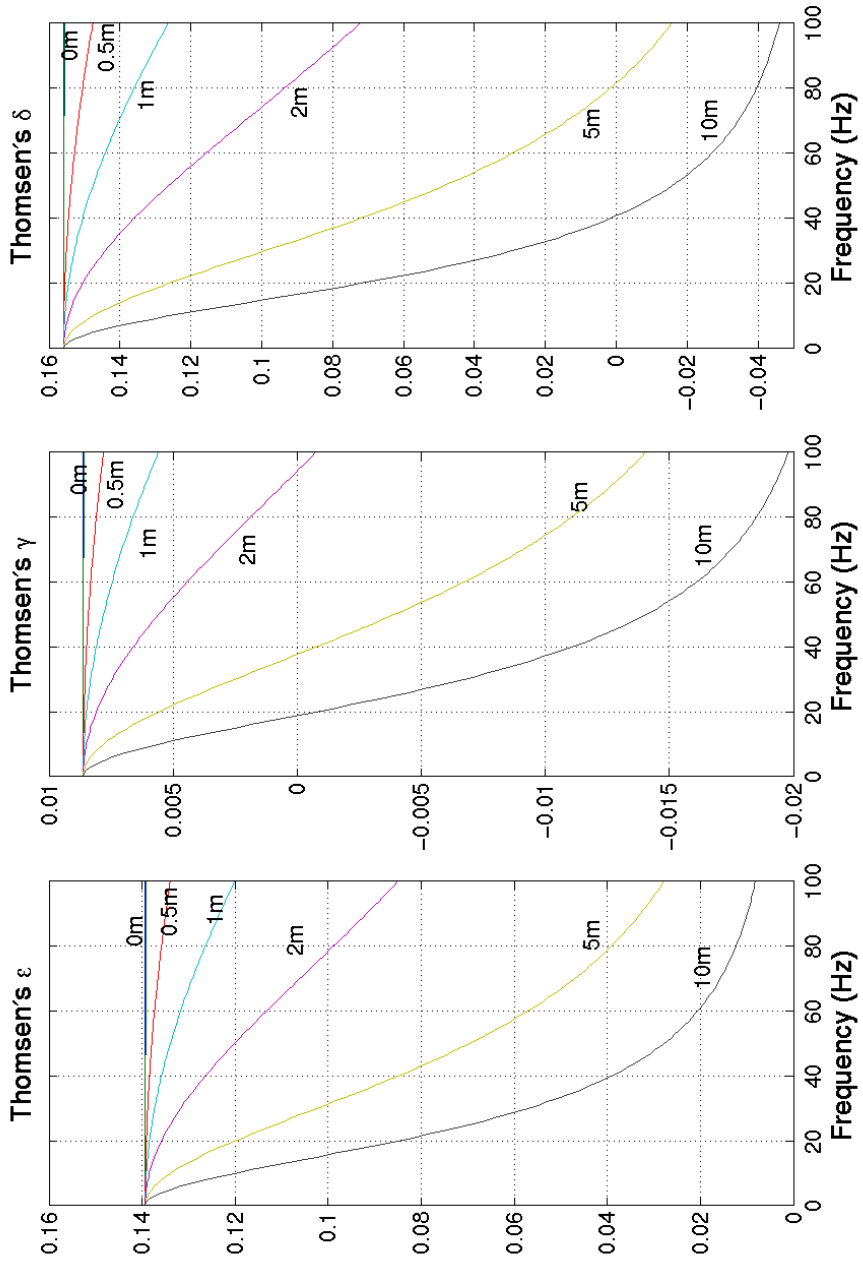

Figure 3. Variation of three Thomsen's anisotropic parameters with frequency computed for different fracture sizes (see text for parameters used).

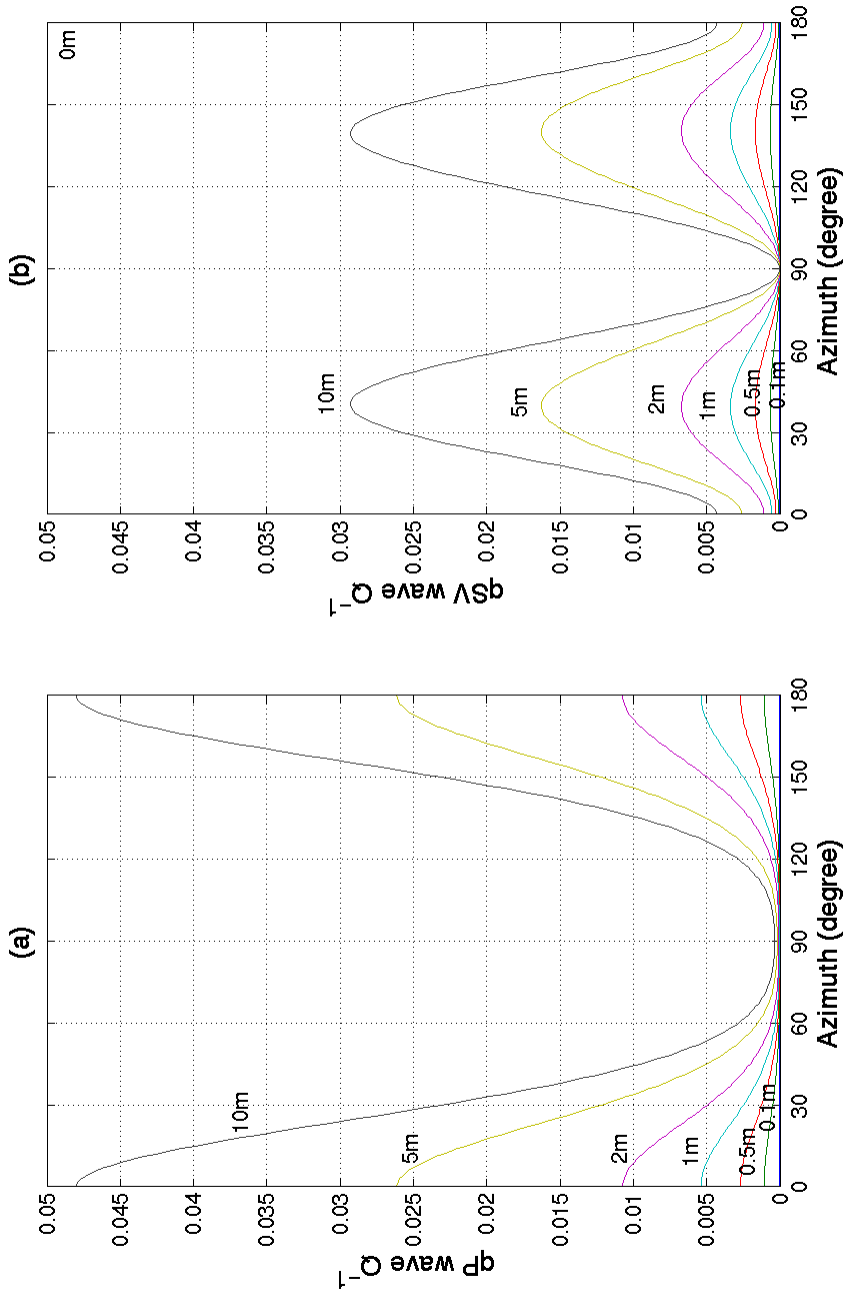

Figure 4. Variations of attenuation Q^{-1} of *qP* and *qSV*-waves with azimuths computed for different fracture sizes.

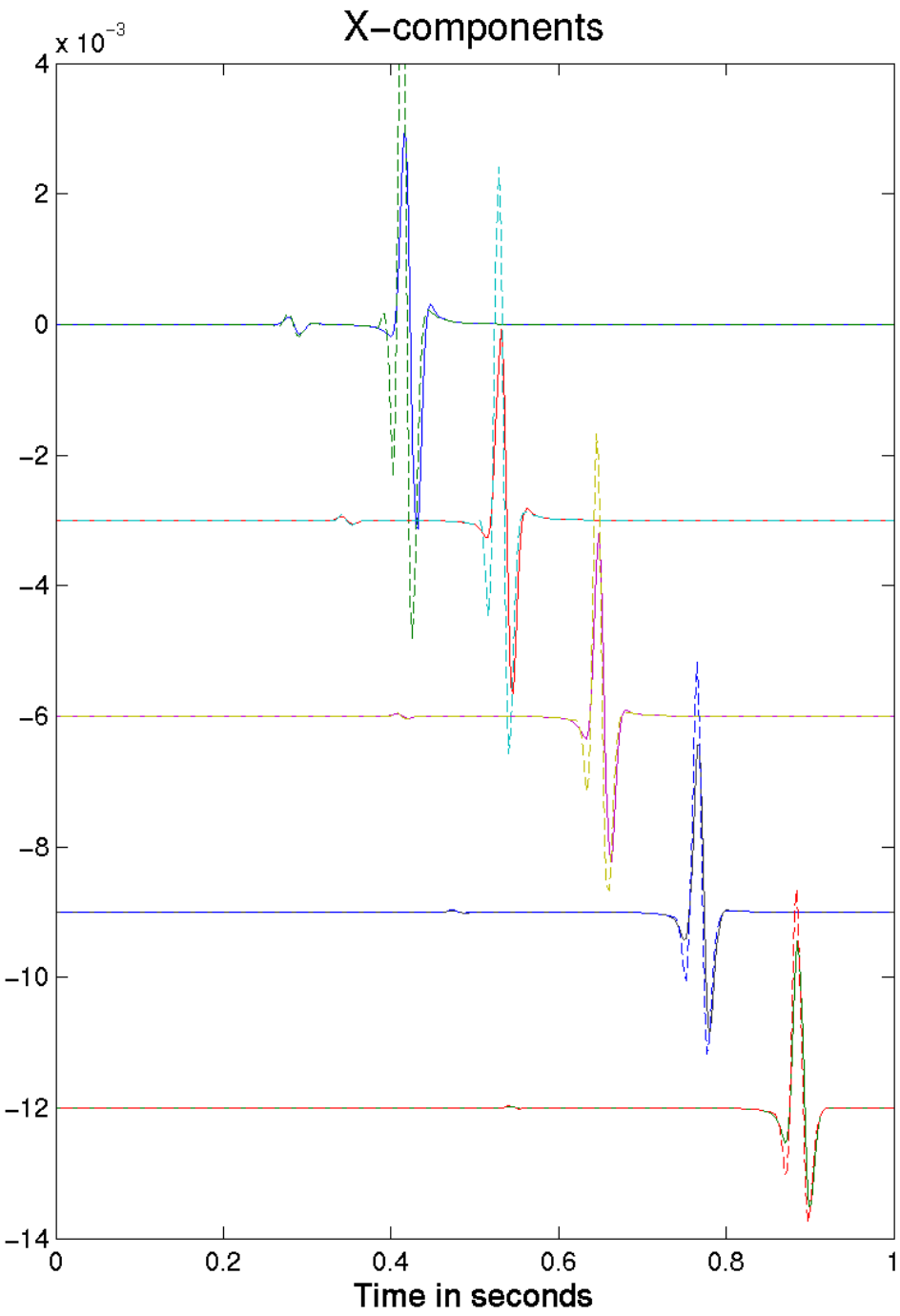

Figure 5. Comparison of synthetic seismograms of the horizontal components for the fracture length of 0.1m (solid lines) and 5m (dashed line). The model is described in the text.

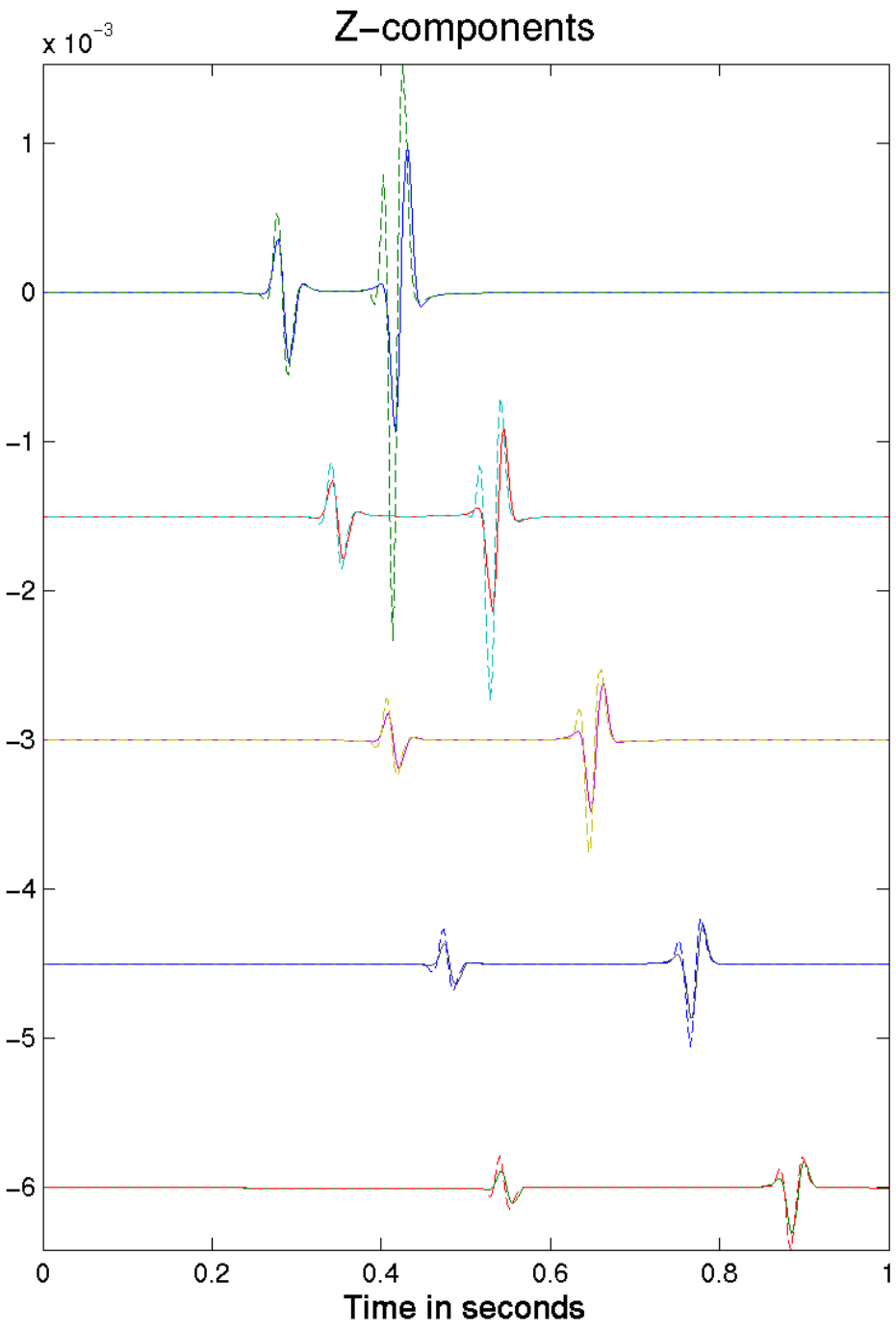

Figure 6. Comparison of synthetic seismograms of the vertical components for the fracture length of 0.1m (solid lines) and 5m (dashed line). The model is described in the text.

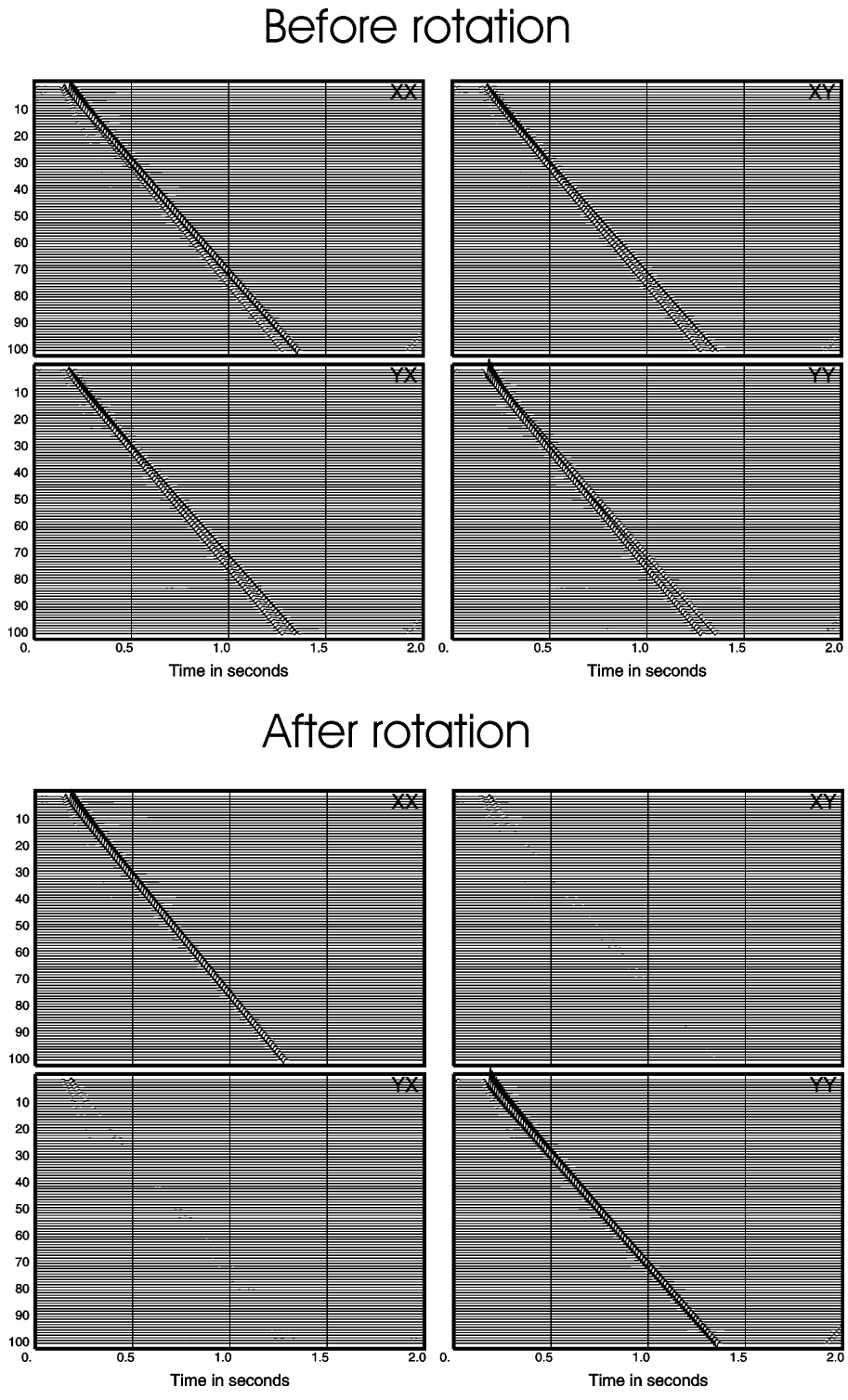

Figure 7. Synthetic four-component data before (top) and after rotation. The top rows with XX and XY are from in-line sources, the bottom rows with YX and YY are from cross-line sources. The first letter denotes the source orientation, and the second the receiver orientation.

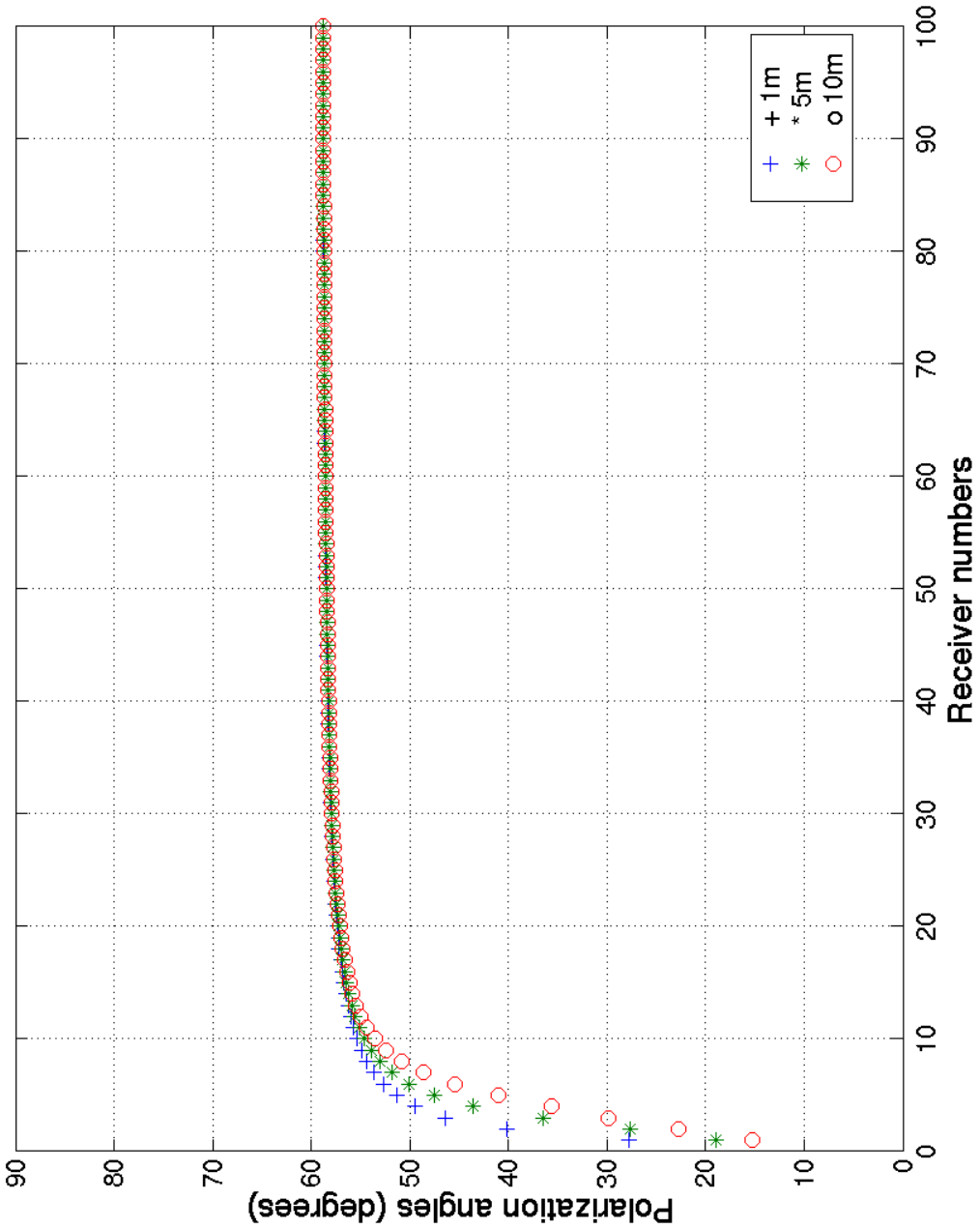

Figure 8. Variations of polarizations of fast split shear-waves with receiver numbers (depth) computed from synthetic four-component data for three different fracture sizes. The angles are relative to the in-line component.

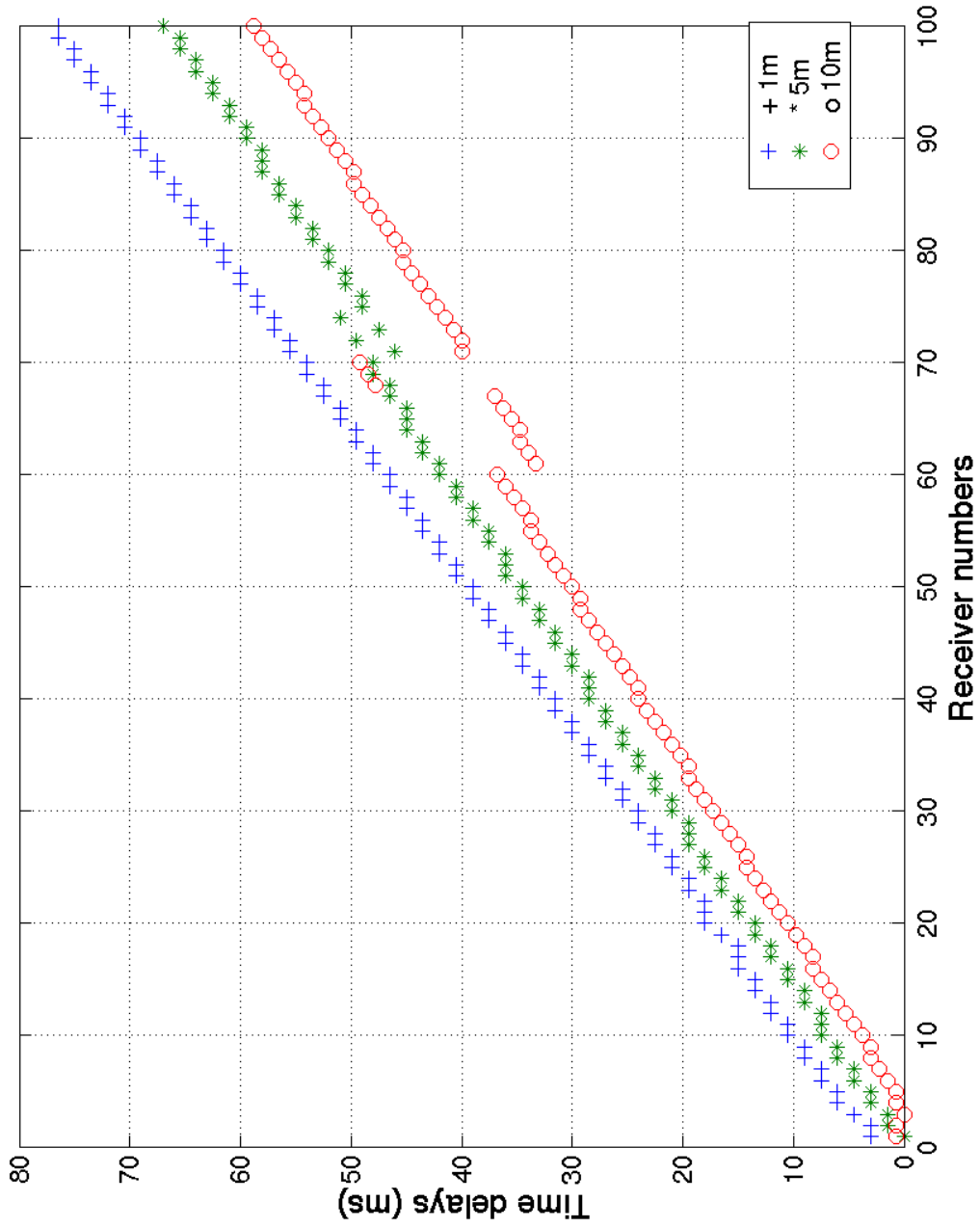

Figure 9. Variations of time-delays of split shear-waves with receiver numbers (depth) computed from synthetic four-component data for three different fracture sizes.

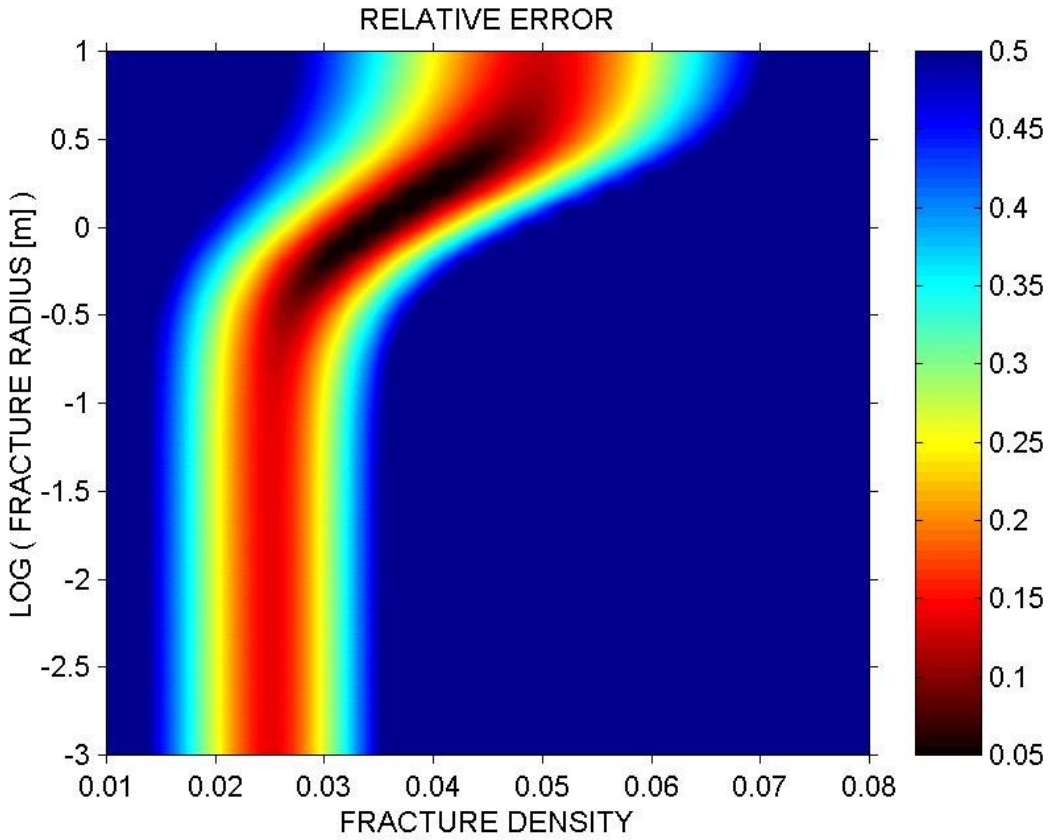

Figure 10. RMS error between predicted and measured time-delay/depth, evaluated over four frequency values for a range of fracture densities and sizes. There is a well-defined minimum, where the error is less than 5%.

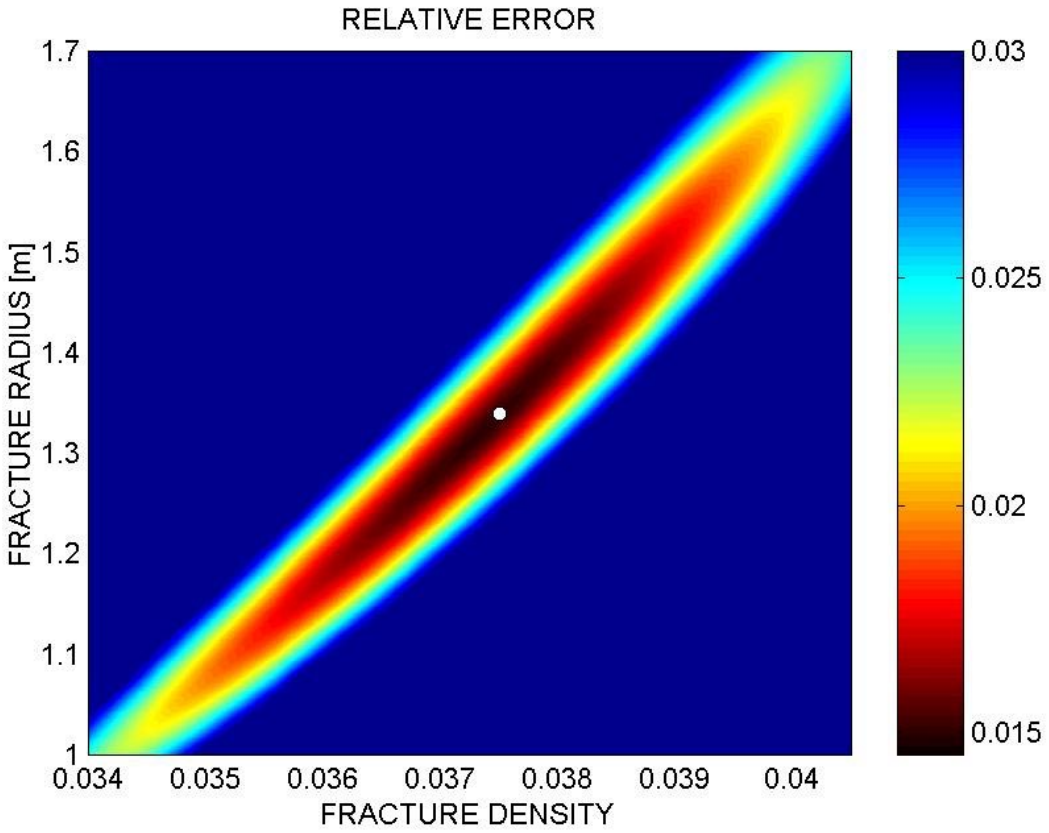

Figure 11. The same as Figure 10 zoomed into the area of small relative error. The white dot indicates the minimum at a fracture density of 0.0375 and a fracture radius of 1.34 m. These values were used to compute frequency dependent elastic coefficients for the Green River formation and generate synthetic data.

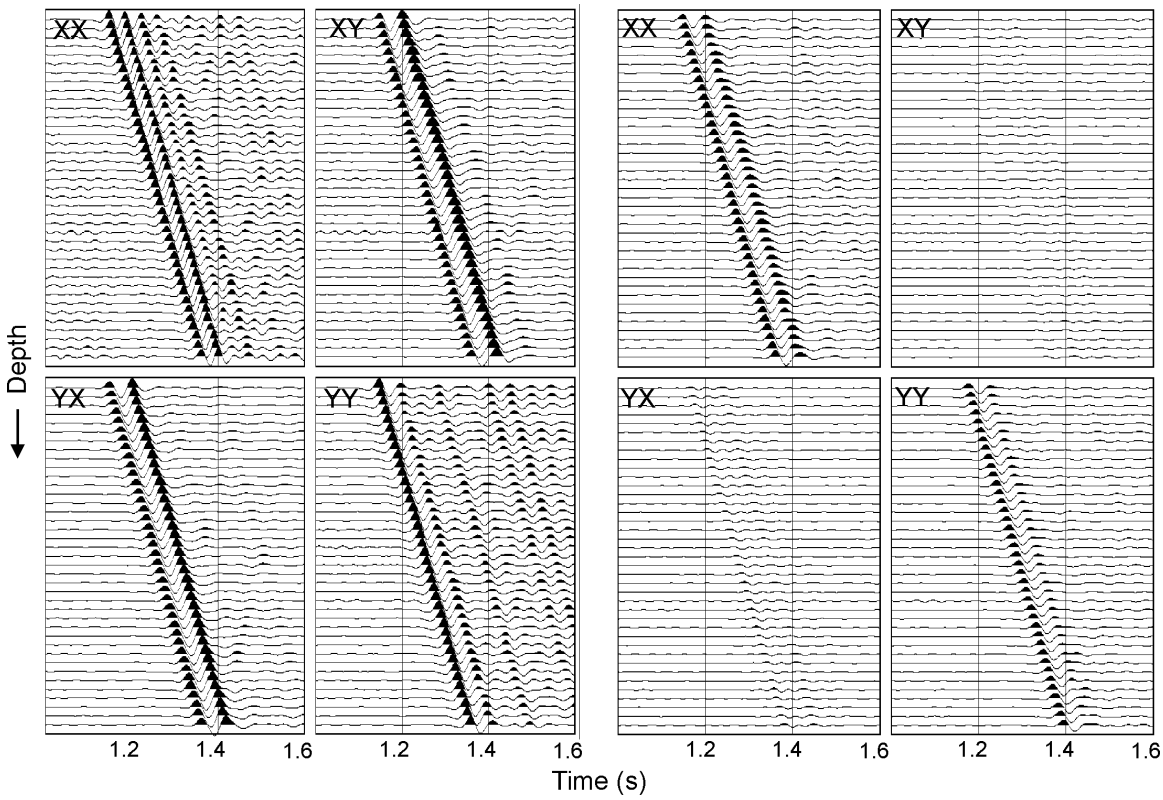

Figure 12: 4C VSP data from the Bluebell Altamont field. Selected traces correspond to the depth interval of the Green River formation. ‘X’ stands for ‘radial’ and ‘Y’ for ‘transverse’; the first letter indicates the source direction and the second one the geophone component. There is strong energy in the crossline components, indicating shear wave splitting in the Green River formation.

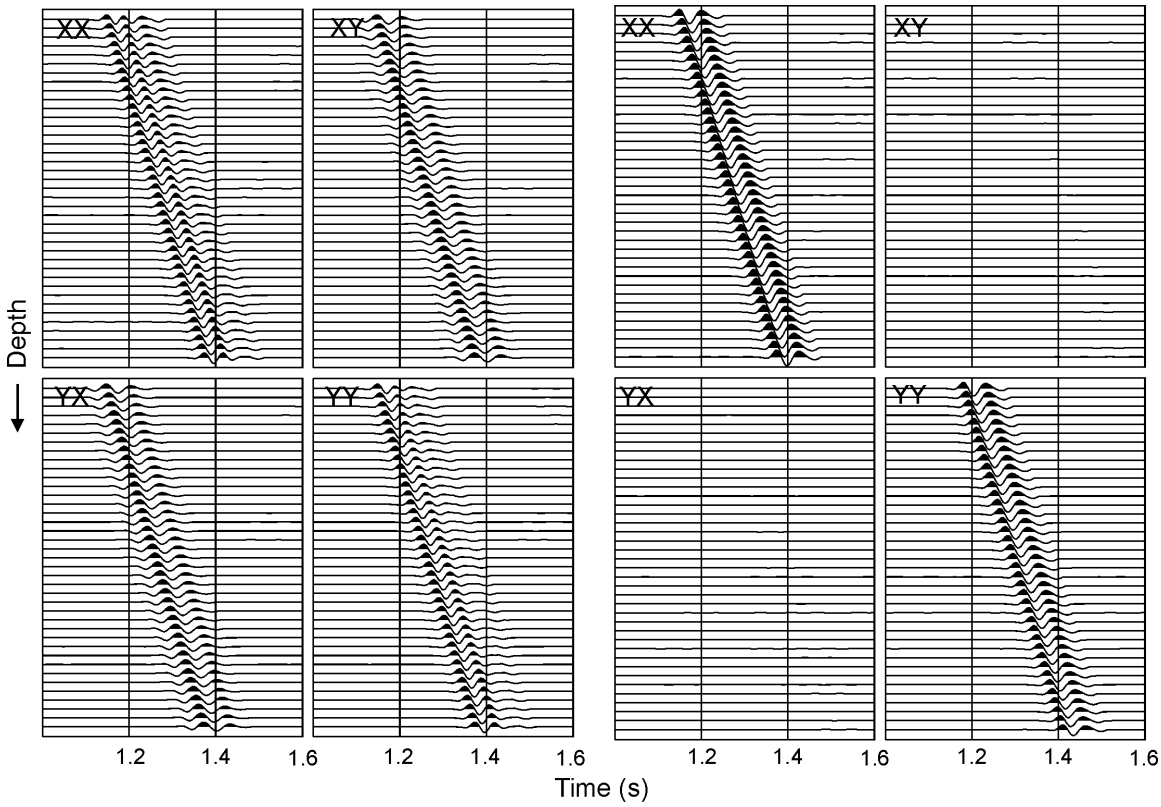

Figure 13: Synthetic 4C data for the Green River formation. The synthetic seismograms correlate well with the real data (compare to Figure 12).

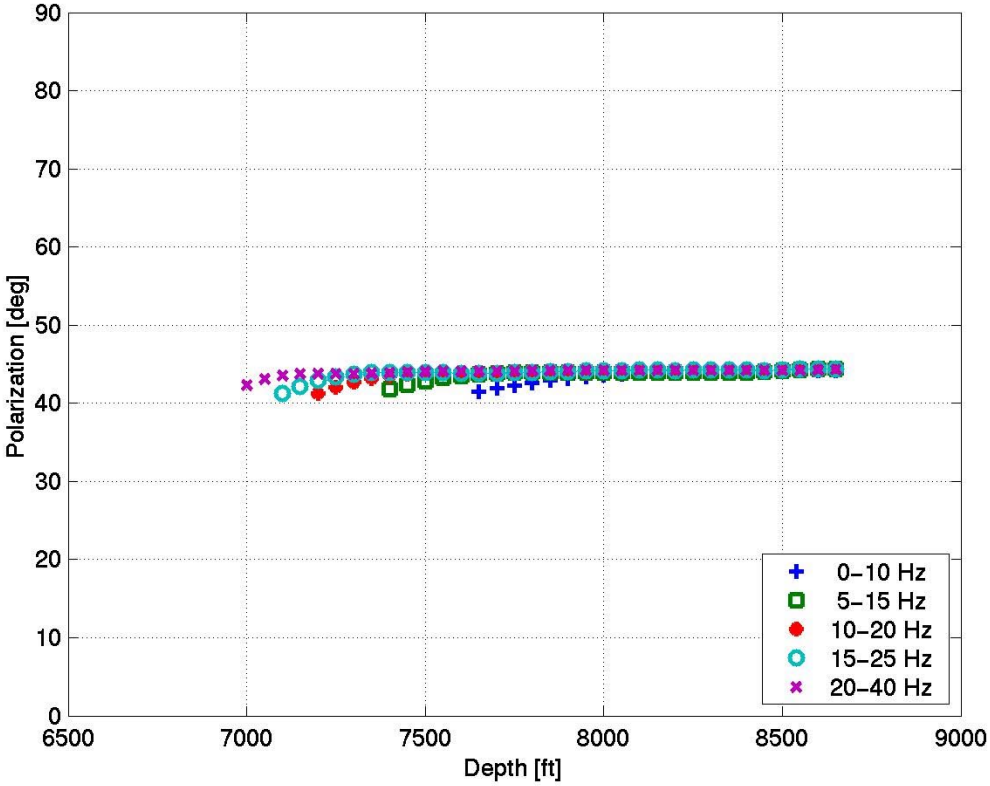

Figure 14. Polarization angles obtained from the synthetics for each frequency band after Alford rotation. The values are almost constant at 44º.

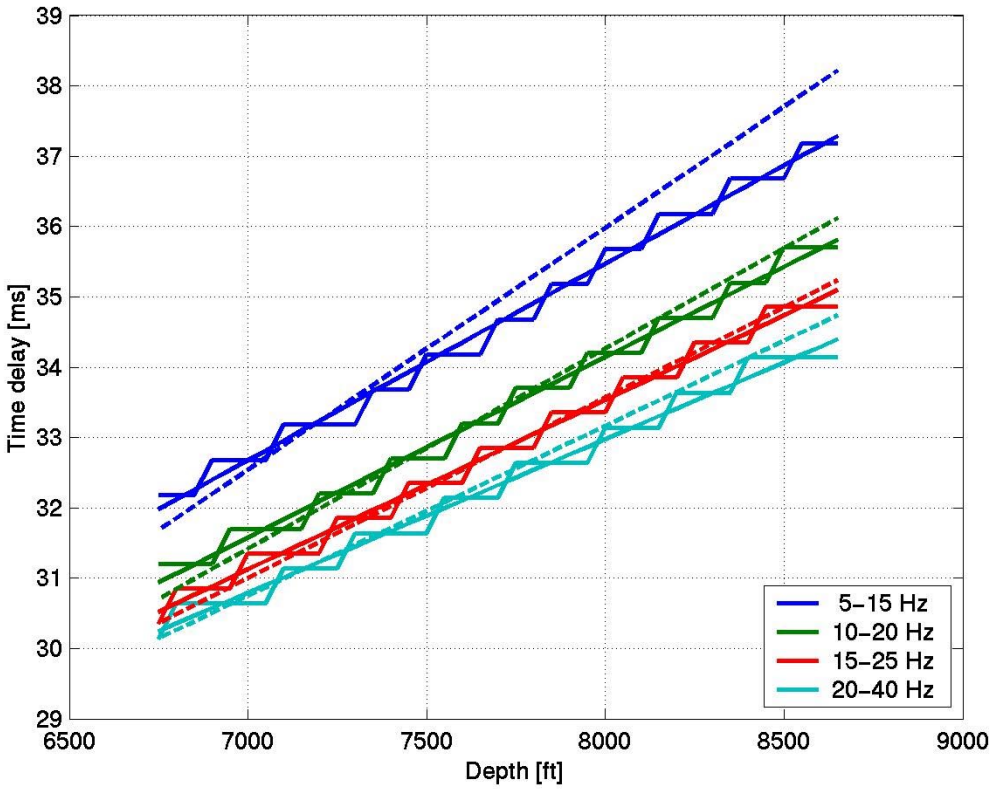

Figure 15. Time-delays estimated from the synthetic data for each frequency band (solid lines) in comparison with the results from the real data (dashed lines). The modelling results match the real data well. The errors are not significant in terms of the estimated values of fracture density and radius. The cause for the slight discrepancy will be a matter of future investigation.